Chemical Science

ROYAL SOCIETY OF CHEMISTRY

EDGE ARTICLE

View Article Online
View Journal | View Issue

Cite this: *Chem. Sci.*, 2023, **14**, 8401

All publication charges for this article have been paid for by the Royal Society of Chemistry

Received 23rd May 2023
Accepted 30th June 2023

DOI: 10.1039/d3sc02599c

rsc.li/chemical-science

Conformationally confined three-armed supramolecular folding for boosting near-infrared biological imaging†

Hui-Juan Wang,[ab] Meng-Meng Zheng,[a] Wen-Wen Xing,[a] Yong-Xue Li,[a] Yao-Yao Wang,[b] Hongjie Zhu,[b] Ying-Ming Zhang,*[a] Qilin Yu*[c] and Yu Liu*[ade]

Herein, a triphenylamine derivative (**TP-3PY**) possessing 4-(4-bromophenyl)pyridine (PY) as an electron-accepting group and tris[*p*-(4-pyridylvinyl)phenyl]amine (TPA) with large two-photon absorption cross-sections as an electron-donating group was obtained, and showed intense absorption in the visible light region (λ_{max} = 509 nm) and weak near-infrared (NIR) fluorescence emission at 750 nm. After complexation with cucurbit[8]uril (CB[8]), **TP-3PY** showed bright NIR fluorescence emission at 727 nm and phosphorescence emission at 800 nm. When the supramolecular assembly (**TP-3PY**⊂CB[8]) further interacted with dodecyl-modified sulfonatocalix[4]arene (SC4AD), the fluorescence and phosphorescence emissions were further enhanced at 710 and 734 nm, respectively. However, only the fluorescence emission of **TP-3PY** was enhanced in the presence of cucurbit[7]uril (CB[7]) and SC4AD. More interestingly, the photoluminescence of **TP-3PY**⊂CB[8]@SC4AD and **TP-3PY**⊂CB[7]@SC4AD assemblies could be excited by both visible (510 nm) and NIR light (930 nm). Finally, these ternary supramolecular assemblies with bright NIR light emission were applied to lysosome imaging of tumor cells and real-time biological imaging of mice.

Introduction

Construction of optical materials through controlling the conformation of molecules is an interesting research field. The common construction strategies are involvement of stimuli-responsive groups, rational design of molecules to tune intermolecular π–π stacking, host–guest interaction and so on.[1–7] The covalent methods often need tedious synthesis, have poor biocompatibility and inevitable biotoxicity. Fortunately, the encapsulation with macrocyclic hosts *via* host–guest interaction can efficiently regulate the molecular conformation and lead to a dramatic makeover of the photophysical properties of guest chromophores.[8,9] Thus, host–guest interaction has been proved to be an efficient method to obtain supramolecular optical materials. In this regard, compared to cucurbit[7]uril (CB[7]), cucurbit[8]uril (CB[8]) possessing a large cavity can encapsulate more than one molecule with high selectivity and binding constants and can lead to the formation of various supramolecular assemblies,[10–13] such as saddle-shaped joints,[14] supramolecular pins,[15] interlocked molecular necklaces,[16] supramolecular network polymers[17] and so on. For instance, Tian and Ma *et al.* reported a triazine derivative with two branches modified by 4-(4-bromophenyl)pyridine (PY), which formed a quaternary stacking structure with tunable photoluminescence after complexation with CB[8].[18] Ni *et al.* reported a type of color-tunable optical material through the reversible conformational changes of supramolecular assemblies.[19] Park *et al.* reported a supramolecular nanoring with high fluorescence yield enhanced by the encapsulation with CB[8].[20] Bhasikuttan *et al.* reported the structure-tuning emissions of coumarin derivatives by changing the conformations after binding to CB[8].[21] Zhao *et al.* reported a triphenylamine derivative (vinyl-pyridinium triphenylamine) to form a three-branched structure after encapsulation by CB[8] which worked as an excellent biological label.[22] Our group also reported a series of phosphorescent molecular foldamers with high phosphorescence yields upon binding with CB[8].[23,24] The excellent optical properties can be attributed to the different

[a]*College of Chemistry, State Key Laboratory of Elemento-Organic Chemistry, Nankai University, Tianjin 300071, China. E-mail: ymzhang@nankai.edu.cn; yuliu@nankai.edu.cn*

[b]*Shandong Provincial Key Laboratory of Chemical Energy Storage and Novel Cell Technology, School of Chemistry and Chemical Engineering, Liaocheng University, Liaocheng 252000, China*

[c]*Key Laboratory of Molecular Microbiology and Technology, College of Life Sciences, Nankai University, Tianjin 300071, China. E-mail: yuqilin@mail.nankai.edu.cn*

[d]*Haihe Laboratory of Sustainable Chemical Transformations (Tianjin), Tianjin 300192, China*

[e]*Collaborative Innovation Center of Chemical Science and Engineering (Tianjin), Tianjin 300072, China*

† Electronic supplementary information (ESI) available: Experimental procedures and characterization. See DOI: https://doi.org/10.1039/d3sc02599c

electronic distributions of chromophores in guest molecules caused by the conformational confinement with the rigid hydrophobic cavity of CB[8].

PY as a star phosphorescent chromophore[25–27] has been widely used to construct anti-counterfeit materials,[28] biological imaging materials[29] and probes.[30] Although more and more aqueous room-temperature phosphorescent materials have been reported, it is still a great challenge to obtain near-infrared (NIR) phosphorescence emission excited by visible or NIR light.[31,32] Herein, we conjugated PY as electron-accepting group to tris[*p*-(4-pyridylvinyl)phenyl]amine (TPA) as an electron-donating group and thus obtained the guest molecule **TP-3PY**, which showed a weak fluorescence emission at 750 nm. After binding with CB[8], enhanced fluorescence emission at 727 nm and weak phosphorescence emission at 800 nm were achieved (Scheme 1). Further, we introduced lower-rim dodecyl-modified sulfonatocalix[4]arene (SC4AD) into the **TP-3PY**⊂CB[8] complex and the ternary assembly showed both bright NIR fluorescence emission (710 nm) and phosphorescence emission (734 nm). The ternary supramolecular assembly was used for tumor cell imaging and optical imaging of mice *in vivo*. In this work, the complexation-induced multiple folding and hierarchical assembling with different macrocycles can be utilized as a co-regulatory strategy for optimizing molecular conformation and photophysical performance.

Results and discussion

Compound **TP-3PY** was obtained through a simple synthetic route (Scheme S1, ESI†) and its corresponding characterization is shown in Fig. S1–S4 (ESI†). Due to the poor solubility of **TP-3PY** in aqueous solution, **A-PY** containing a single PY arm was synthesized as a reference compound. The synthetic route and corresponding characterization of **A-PY** are shown in Scheme S2 and Fig. S5–S7 (ESI†). First, we investigated the assembling mode of **TP-3PY**⊂CB[8]. Considering that the CB[8] with a larger cavity can bind two pyridinium moieties and **TP-3PY** possesses six positively charged pyridinium groups, the binding ratio between **TP-3PY** and CB[8] was explored by UV/vis absorption spectra. The Job plot indicated that the CB[8] encapsulated **TP-3PY** with a ratio of 3 : 1 (Fig. 2d). As shown in Scheme 2, there are three possible binding modes of **TP-3PY**⊂CB[8] assembly: (1) molecular foldamer with a 1 : 3 ratio, (2) dimer formed by molecular stacking with a 2 : 6 ratio, and (3) supramolecular polymer networks with an $n : 3n$ ratio. In view of the dimer mode with a 2 : 6 ratio being an H-aggregate which is a poor emitter accompanying photoluminescence quenching,[8] the dimer assembly mode was tentatively excluded. Moreover, the aggregate sizes of **TP-3PY**, **TP-3PY**⊂CB[8] and **TP-3PY**⊂CB[7] were evaluated by diffusion ordered spectroscopy (DOSY) in aqueous solution. As shown in Fig. S11 (ESI†), when the concentration of **TP-3PY** was fixed as 0.3 mM, the diffusion coefficients of **TP-3PY**, **TP-3PY**⊂CB[8] and **TP-3PY**⊂CB[7] were calculated to be 1.86×10^{-10} m^2 s^{-1}, 1.55×10^{-10} m^2 s^{-1} and 1.49×10^{-10} m^2 s^{-1}, respectively. The higher diffusion coefficient of **TP-3PY**⊂CB[8] than **TP-3PY**⊂CB[7] indicated that there was no supramolecular polymer formed in the assembly of **TP-3PY**⊂CB[8]. Thus, the polymer assembly mode was ruled out. To confirm the molecular folding conformation of **TP-3PY**⊂CB[8], a series of ^{1}H NMR spectra were recorded. The binding behaviors of **TP-3PY**⊂CB[8] were investigated by ^{1}H NMR spectroscopy, revealing that the aromatic protons of **TP-3PY** shifted upfield after binding with CB[8] (Fig. 1). To give more details of the binding mode, 2D rotating-frame

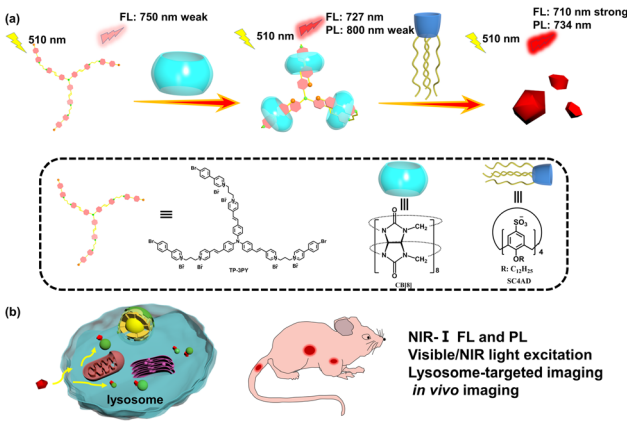

Scheme 1 (a) Schematic diagram of the ternary supramolecular assembly TP-3PY⊂CB[8]@SC4AD with NIR fluorescence and phosphorescence emission. (b) Applications of TP-3PY⊂CB[8]@SC4AD (FL: fluorescent luminescence, PL: phosphorescent luminescence).

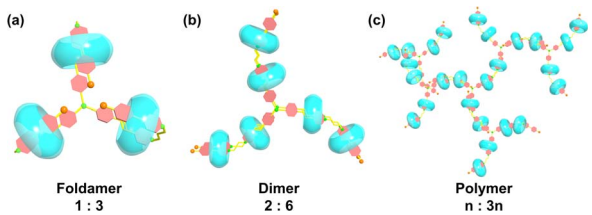

Scheme 2 Schematic diagram of three possible binding modes of TP-3PY⊂CB[8].

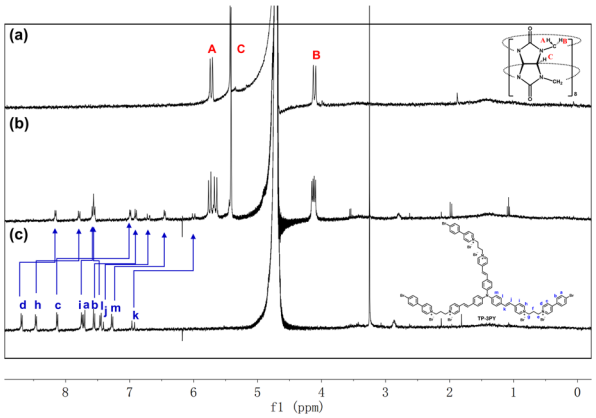

Fig. 1 ^{1}H NMR spectra of (a) CB[8], (b) TP-3PY⊂CB[8] and (c) TP-3PY ([TP-3PY] = 3×10^{-4} M, [CB[8]] = 9×10^{-4} M, 400 MHz, D_2O, 298 K).

Overhauser effect spectroscopy (ROESY) of **TP-3PY**⊂CB[8] was employed. There are strong correlated signals between H_b and H_i, H_l, H_a and H_m (Fig. S10, ESI†) indicating the possible assembly mode of the molecular folding conformation with a 1 : 3 ratio. To further confirm the assembling mode, the assembly mode of **A-PY**⊂CB[8] was explored. First, the binding stoichiometry of **A-PY**⊂CB[8] was confirmed by the mass spectrum and Job plot of **A-PY**⊂CB[8], giving evidence of the 1 : 1 binding ratio (Fig. S12, ESI†). As shown in Fig. S13 (ESI†), all the protons of **A-PY** shifted to higher field except for the styrylpyridinium protons (H_8, H_9) and the alkyl protons (H_5, H_6 and H_7) after binding with CB[8]. And the protons of CB[8] split into two double peaks, indicating the different chemical environments, which excluded the linear polymer formed by the head-to-tail binding mode. Therefore, we speculated that the **A-PY**⊂CB[8] formed a folded conformation. Further, the ROESY of **A-PY**⊂CB[8] was performed and some significant correlations between H_8 and H_3, as well as H_4 and H_9 were observed (Fig. S16, ESI†). The intramolecular correlation suggested that the distance between the phenylpyridine group and the styrylpyridine group became shorter, which means the folded molecular conformation of **A-PY** was caused by the encapsulation of CB[8]. All the evidence above indicated that the binding mode of **TP-3PY**⊂CB[8] adopted a three-armed folded conformation. We also simulated the structure of supramolecular assembly **TP-3PY**⊂CB[8] (Fig. S19, ESI†) and further confirmed the triple foldamer conformation.

Further, the assembling behaviors of **TP-3PY**⊂CB[8] were investigated by UV/vis absorption spectra. As shown in Fig. 2a, the UV/vis absorption spectrum of **TP-3PY** showed peaks at around 315 nm and 509 nm, which were assigned to the PY moiety and the TPA moiety, respectively. Upon the addition of different equivalents of CB[8] to the solution of **TP-3PY**, the peaks around 315 nm and 509 nm showed a bathochromic shift to 332 nm and 556 nm, respectively. The color of the solution changed from red to purple to blue (Fig. 2b), which evidenced the formation of J-aggregates in **TP-3PY**⊂CB[8].[33] This phenomenon also implied the formation of a strong charge transfer (CT) assembly upon binding with CB[8]. Based on the above observations, we speculated that the encapsulation of CB[8] can enhance the electron-withdrawing effect of pyridinium from TPA by neutralizing its positive charge. As a reference host molecule, 6 equivalents of CB[7] were added into the aqueous solution of **TP-3PY**. And the UV/vis absorption spectrum of **TP-3PY**⊂CB[7] showed a slight red shift compared to **TP-3PY** (Fig. S20b, ESI†). Moreover, the association constant between **TP-3PY** and CB[8] was calculated to be 5.98×10^{22} M^{-3} (Fig. 2c) based on the UV/vis absorption spectroscopic titration. The association constant between reference molecule **A-PY** and CB[8] was also calculated using the same method ($K_s = 8.1 \times 10^6$ M^{-1}, Fig. S12b, ESI†).

Photoluminescence experiments of **TP-3PY** after assembling with CB[8] were explored. As shown in Fig. 3a, the photoluminescence emission of **TP-3PY** at 750 nm shifted to 727 nm and increased upon titration with CB[8] in aqueous solution. Upon titration with CB[8], the phosphorescence

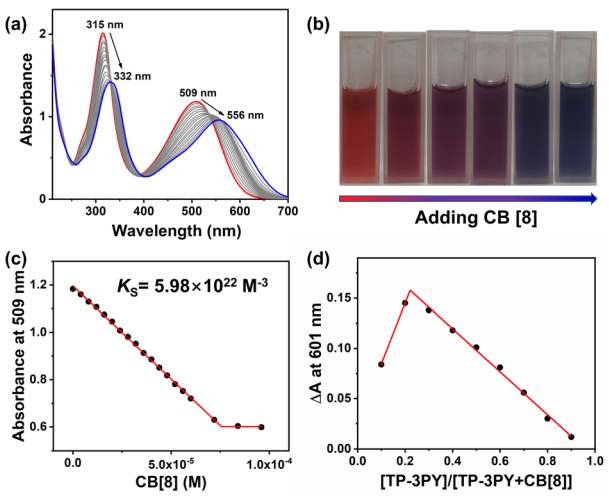

Fig. 2 (a) UV/vis absorption spectra and (b) photographs of **TP-3PY** (2×10^{-5} M) with different concentrations of CB[8] (0–96 μM), (c) the nonlinear least-squares analysis of the variation of absorbance at 509 nm with the concentrations of CB[8] to calculate the binding constant from the corresponding absorbance in (a). (d) Job plot according to the method for continuous variations, indicating 3 : 1 stoichiometry for CB[8] and **TP-3PY** ([CB[8]] + [**TP-3PY**] = 2.083×10^{-5} M).

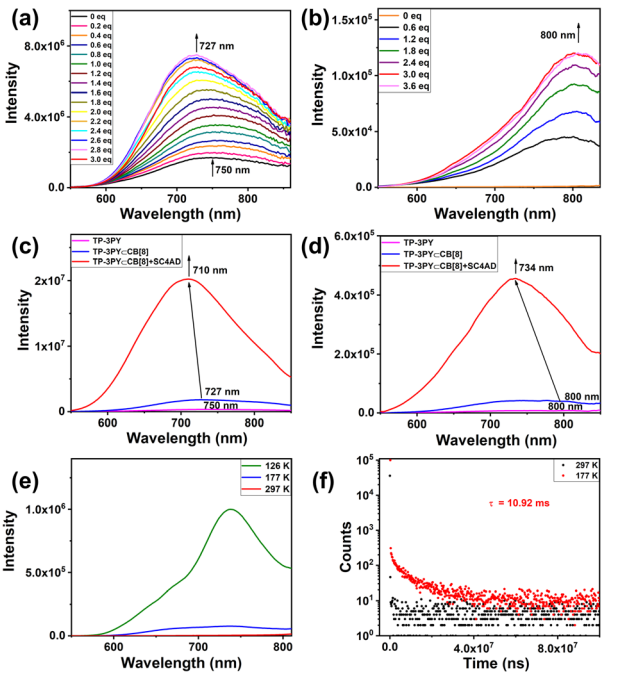

Fig. 3 (a) Photoluminescence emission spectra and (b) phosphorescence emission spectra (delayed 50 μs) of **TP-3PY** (2×10^{-5} M) with different concentrations of CB[8] (0–60 μM, λ_{ex} = 510 nm, 298 K), (c) photoluminescence emission spectra and (d) phosphorescence emission spectra (delayed 50 μs) of **TP-3PY**, **TP-3PY**⊂CB[8] and **TP-3PY**⊂CB[8]@SC4AD ([**TP-3PY**] = 2×10^{-5} M, [CB[8]] = 6×10^{-5} M, [SC4AD] = 4×10^{-5} M, λ_{ex} = 510 nm, 298 K). (e) Phosphorescence emission spectra (delayed 50 μs) and (f) time-resolved PL decay curves of **TP-3PY**⊂CB[8] at different temperatures ([**TP-3PY**] = 2×10^{-5} M, CB[8] = 6×10^{-5} M, λ_{ex} = 510 nm).

emission spectra (delayed 50 μs) of **TP-3PY** showed a weak peak at 800 nm and increased gradually and reached the maximum with 3 equivalents of CB[8] (Fig. 3b). To further enhance the photoluminescence intensity, the amphipathic sulfonatocalix[4]arene (SC4AD) was introduced into the **TP-3PY**⊂CB[8] to form a ternary supramolecular assembly. The photoluminescence emission of **TP-3PY**⊂CB[8] at 727 nm shifted to 710 nm and increased 11-fold with the addition of 2 equivalents of SC4AD (Fig. S21a, ESI†). The phosphorescence emission spectra (delayed 50 μs) of **TP-3PY**⊂CB[8] at 800 nm shifted to 734 nm. The time-resolved phosphorescence decay curves of **TP-3PY**⊂CB[8] and **TP-3PY**⊂CB[8]@SC4AD are shown in Fig. S22 (ESI†), giving the phosphorescence lifetimes of 4.59 μs (800 nm) and 4.26 μs (730 nm), respectively. The fluorescence lifetimes of **TP-3PY**, **TP-3PY**⊂CB[8] and **TP-3PY**⊂CB[8]@SC4AD were determined to be 0.8 ns (750 nm), 2.66 ns (730 nm) and 1.16 ns (710 nm), respectively (Fig. S22, ESI†). To further confirm the photophysical properties of the emission peak of **TP-3PY**⊂CB[8] at 800 nm and the emission peak of **TP-3PY**⊂CB[8]@SC4AD at 734 nm, the photoluminescence experiments (delayed 50 μs) of **TP-3PY**⊂CB[8] and **TP-3PY**⊂CB[8]@SC4AD were performed at different temperatures. As shown in Fig. 3 and S21 (ESI†), both the intensity and lifetime of the long-lived emission enhanced greatly when the temperature reached 126 K and 177 K, which is consistent with the view that the non-radiative relaxation from the triplet to the ground state could be suppressed at low temperature.[34] As a control, the fluorescence spectra of **TP-3PY** were measured with different concentrations of CB[7]. The results indicated a blue shift of the fluorescence maximum peak from 750 nm to 690 nm, due to the weakened CT effect caused by the increased distance between the donor and acceptor (Fig. S23a, ESI†). Similarly, the introduction of SC4AD caused a large enhancement of the fluorescence intensity of **TP-3PY**⊂CB[7] (Fig. S23b, ESI†). Compared to our previous work,[35] this ternary supramolecular assembly showed fluorescence and phosphorescence emissions in the NIR-I region (700–900 nm), which is more suitable for biological imaging[36] (Fig. S24, ESI†). Subsequently, the assembling behaviors were investigated by dynamic light scattering (DLS), ζ potential, and transmission electron microscopy (TEM) experiments. As shown in Fig. S17 and S18 (ESI†), both **TP-3PY**⊂CB[7]@SC4AD and **TP-3PY**⊂CB[7]@SC4AD formed negatively charged fragments with diameter of hundreds of nanometers.

It was reported that TPA possesses large two-photon absorption cross sections.[37,38] The UV/vis absorption of **TP-3PY** in different solvents and density functional theory (DFT) calculations (Fig. 4a) were implemented to shed light on the inherent intramolecular charge transfer (ICT) of **TP-3PY**. The solvent-dependent absorbance implied the internal charge transfer nature of **TP-3PY** upon excitation (Fig. S25, ESI†). The occupied molecular orbital is mainly localized at the TPA core, and the unoccupied molecular orbital is localized at the PY branches, indicating electron transfer from TPA to PY may occur as **TP-3PY** is excited.[39] We speculated that the ternary supramolecular assemblies **TP-3PY**⊂CB[8]@SC4AD with strong NIR-I emission may have the property of two-photon

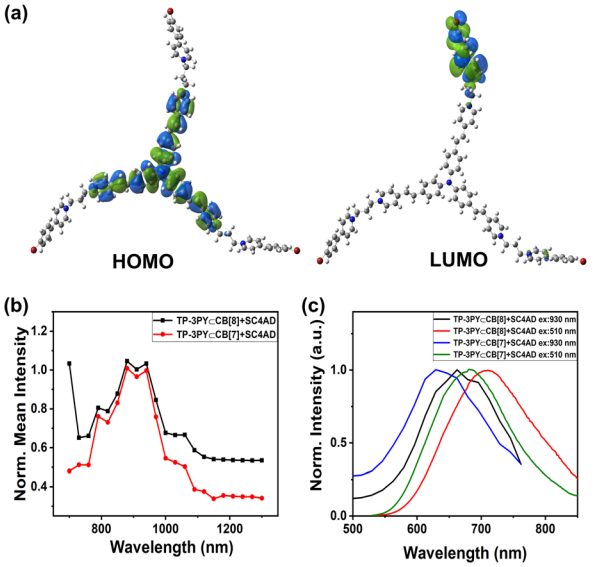

Fig. 4 (a) HOMO/LUMO of **TP-3PY**. (b) Two-photon excitation spectra and (c) photoluminescence emission spectra of **TP-3PY**⊂CB[8]@SC4AD and **TP-3PY**⊂CB[7]@SC4AD.

absorption. As expected, the ternary assemblies **TP-3PY**⊂CB[8]@SC4AD and **TP-3PY**⊂CB[7]@SC4AD could reach maximal NIR emission with the femtosecond laser excitation wavelength ranging from 760 to 1200 nm (Fig. 4b). Further, upon the excitation at 930 nm with a femtosecond laser, the fluorescence spectra of **TP-3PY**⊂CB[8]@SC4AD and **TP-3PY**⊂CB[7]@SC4AD showed a similar spectral band and position with one-photon excitation at 510 nm (Fig. 4c). The visible and NIR light excitation property can endow the ternary supramolecular assembly with features of higher penetrability in tissue and lower phototoxicity.[40,41]

By virtue of the above functional characteristics of the ternary supramolecular assembly **TP-3PY**⊂CB[8]@SC4AD, we applied it to the targeted imaging of HeLa cells and *in vivo* bioimaging of mice. First, the cytotoxicity experiments of **TP-3PY**⊂CB[8]@SC4AD were evaluated by cell counting kit-8 (CCK-8) assay with HeLa cells as a model. HeLa cells were treated with various concentrations of **TP-3PY**⊂CB[8]@SC4AD (from 0 to 25 μM) for 24 h and then the cell viability was measured by a standard CCK-8 assay. The results of cell cytotoxicity experiments showed that the ternary supramolecular assembly **TP-3PY**⊂CB[8]@SC4AD showed negligible cytotoxicity even when the concentration reached 25 μM (Fig. S26, ESI†). Further, confocal laser scanning microscopy (CLSM) experiments were executed to observe the distribution of **TP-3PY**⊂CB[8]@SC4AD in cells. HeLa cells were treated with **TP-3PY**⊂CB[8]@SC4AD for 12 h. Then, the HeLa cells were co-incubated with Mito-Tracker Green or Lyso-Tracker Green for 30 min. Subsequently, the CLSM experiments were performed to observe the intracellular distribution of the ternary supramolecular assembly. As shown in Fig. 5, bright NIR luminescence could be observed in a red channel (650–750 nm) in cells when excited by a 488 nm laser.

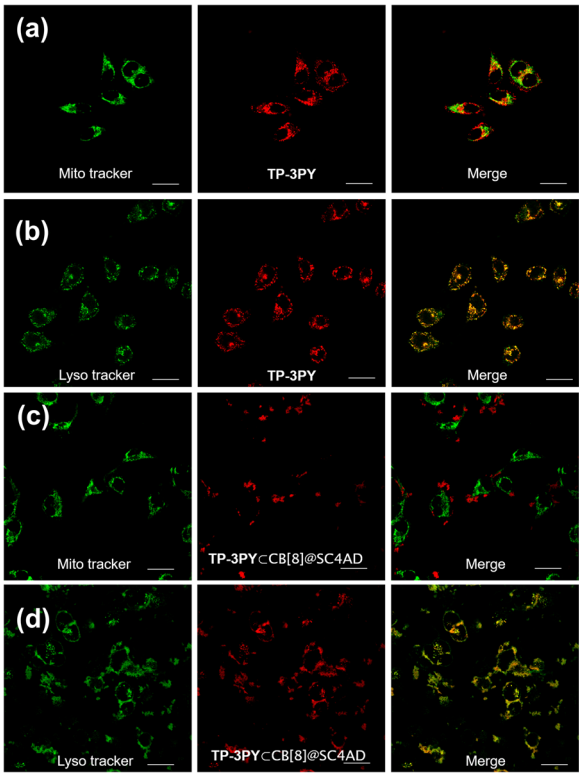

Fig. 5 CLSM images of HeLa cells co-stained with **TP-3PY** (2×10^{-5} M) and (a) Mito Tracker Green and (b) Lyso Tracker Green, respectively. CLSM images of HeLa cells co-stained with **TP-3PY**⊂CB[8]@SC4AD ([**TP-3PY**] $= 2 \times 10^{-5}$ M, [CB[8]] $= 6 \times 10^{-5}$ M, [SC4AD] $= 6 \times 10^{-5}$ M) and (c) Mito Tracker Green and (d) Lyso Tracker Green, respectively. The emission of **TP-3PY** and **TP-3PY**⊂CB[8]@SC4AD was obtained using excitation at 488 nm. Scale bar: 30 μm.

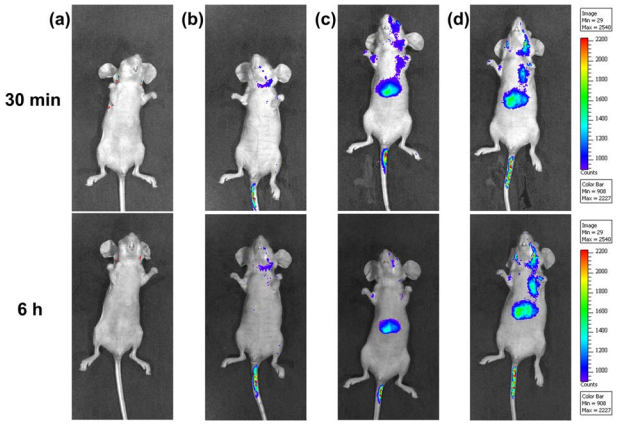

Fig. 6 *In vivo* bioimaging of the mice after injection of (a) saline, (b) **TP-3PY**, (c) **TP-3PY**⊂CB[8]@SC4AD and (d) **TP-3PY**⊂CB[7]@SC4AD for 30 min (up) and 6 h (down) ($\lambda_{ex} = 510$ nm, optical imaging windows in Cy5.5 mode, 298 K).

Further, colocalization assays were executed to observe the subcellular distribution of **TP-3PY**⊂CB[8]@SC4AD. As shown in Fig. 5d, the NIR emission of **TP-3PY**⊂CB[8]@SC4AD monitored from 650 nm to 750 nm showed good overlapping with Lyso-Tracker Green (Pearson's correlation coefficient, $\rho = 0.91$) (Fig. S28, ESI†), indicating that **TP-3PY**⊂CB[8]@SC4AD could preferentially accumulate in lysosome. In the control group, no obvious overlapping between the NIR emission and Mito-Tracker Green was observed (Fig. 5c), implying that the ternary supramolecular assembly was not accumulated in mitochondria. For comparison, the same cell imaging experiments were executed using **TP-3PY** and **TP-3PY**⊂CB[7]@SC4AD. Experimental results showed that both **TP-3PY** and **TP-3PY**⊂CB[7]@SC4AD overlapped with Lyso-Tracker Green (Fig. 5 and S27, ESI†) with high Pearson's correlation coefficients, $\rho = 0.85$ and 0.67, respectively (Fig. S28, ESI†).

Benefiting from the bright NIR emission excited by visible light of the ternary supramolecular assemblies (**TP-3PY**⊂CB[8]@SC4AD, **TP-3PY**⊂CB[7]@SC4AD), real-time *in vivo* imaging of intact animals was implemented using a nude mouse model. The **TP-3PY**⊂CB[8]@SC4AD and **TP-3PY**⊂CB[7]@SC4AD were injected intravenously into the tail vein of nude mice, respectively, and then the images were scanned at different time points using an *in vivo* imaging system. The control groups were injected with saline and **TP-3PY**, respectively. Considering the inspiring imaging of the assembly in live cells and its ideal NIR-I optical imaging window, the fluorescence of the mice was monitored after the injection for 30 min and 6 h. In the two control groups (*i.e.*, the groups injected with saline or **TP-3PY**), the mice exhibited no or only quite low levels of emitted fluorescence (Fig. 6a and b). In contrast, as depicted in Fig. 6c, after 30 min injection, the NIR-I emission signal of **TP-3PY**⊂CB[8]@SC4AD ($\lambda_{em} = 710$ nm) was clearly observed *in vivo*, which has preferential accumulation in the liver and lymph nodes, indicating an excellent NIR-I imaging ability of the assembly. When it comes to **TP-3PY**⊂CB[7]@SC4AD, the NIR-I emission was stronger and more durable (Fig. 6d). These results suggested that the enhanced NIR-I emission caused by the cascade assembly made the real-time imaging of intact animals possible.

Conclusions

In summary, we have developed a ternary supramolecular assembly constructed by the three armed folding of **TP-3PY**⊂CB[8] and further assembled with SC4AD in water, which showed bright NIR-I fluorescence emission and room-temperature phosphorescence emission. **TP-3PY** showed very weak fluorescence emission at 750 nm, which was too weak to be used for optical imaging of animals *in vivo*. After the first assembling with CB[8], the intensity of the NIR-I emission of fluorescence was enhanced and phosphorescence emission appeared. After introducing of amphipathic SC4AD, the NIR-I emission of fluorescence and phosphorescence was subsequently enhanced. In contrast, the photophysical behaviors of **TP-3PY** after assembling with CB[7] were investigated. When complexed with CB[7], the fluorescence emission of **TP-3PY** shifted to 690 nm and the intensity was enhanced greatly. Further introduction of SC4AD caused a secondary enhancement of the fluorescence emission intensity at 690 nm. Considering the large two-photon

absorption cross-sections of TPA derivatives, the ternary **TP-3PY**⊂CB[8]@SC4AD and **TP-3PY**⊂CB[7]@SC4AD assemblies could be excited at 930 nm with a femtosecond laser, and the fluorescence spectra of **TP-3PY**⊂CB@SC4AD and **TP-3PY**⊂CB[7]@SC4AD showed a similar spectral band and position with one-photon excitation at 510 nm. Furthermore, the ternary supramolecular assemblies were successfully used for optical imaging of HeLa cell lysosome and mice *in vivo*. Our work demonstrates the power of supramolecularly conformational confinement, which can be developed as a feasible strategy for obtaining highly compatible and efficient bioimaging agents.

Data availability

Data supporting this article have been uploaded as ESI.†

Author contributions

The manuscript was written through contributions of all authors. All authors have given approval to the final version of the manuscript.

Conflicts of interest

There are no conflicts to declare.

Acknowledgements

This work was financially supported by the National Natural Science Foundation of China (grant no. 22131008 and 22171148) and the Fundamental Research Funds for the Central Universities. We also thank the Haihe Laboratory of Sustainable Chemical Transformations for financial support. All experimental procedures were performed in compliance with the relevant laws and institutional guidelines, and were approved and in accordance with China's National Code of Animal Care for Scientific Experimentation. The experiments were also assessed by the Animal Experimentation Ethics Committee of Nankai University, and the assigned approval number is 2021-SYDELL-000448.

References

1 J. Yang, M. Fang and Z. Li, *Acc. Mater. Res.*, 2021, **2**, 644–654.
2 H. Chen, B. Dong, Y. Tang and W. Lin, *Acc. Chem. Res.*, 2017, **50**, 1410–1422.
3 Q. Li and Z. Li, *Acc. Chem. Res.*, 2020, **53**, 962–973.
4 C. Wang, W. Chi, Q. Qiao, D. Tan, Z. Xu and X. Liu, *Chem. Soc. Rev.*, 2021, **50**, 12656–12678.
5 H.-J. Wang, H.-Y. Zhang, W.-W. Xing, H. Wu, Y.-L. Cui and Y. Liu, *Chin. Chem. Lett.*, 2022, **33**, 4033–4036.
6 S. Garain, S. N. Ansari, A. A. Kongasseri, B. Chandra Garain, S. K. Pati and S. J. George, *Chem. Sci.*, 2022, **13**, 10011–10019.
7 S. Garain, S. M. Wagalgave, A. A. Kongasseri, B. C. Garain, S. N. Ansari, G. Sardar, D. Kabra, S. K. Pati and S. J. George, *J. Am. Chem. Soc.*, 2022, **144**, 10854–10861.
8 H. Nie, Z. Wei, X. L. Ni and Y. Liu, *Chem. Rev.*, 2022, **122**, 9032–9077.
9 S. K. Bhaumik, R. Biswas and S. Banerjee, *Chem.–Asian J.*, 2021, **16**, 2195–2210.
10 G. Wu, M. Olesińska, Y. Wu, D. Matak-Vinkovic and O. A. Scherman, *J. Am. Chem. Soc.*, 2017, **139**, 3202–3208.
11 M. Olesińska, G. Wu, S. Gómez-Coca, D. Antón-García, I. Szabó, E. Rosta and O. A. Scherman, *Chem. Sci.*, 2019, **30**, 1809–1814.
12 W.-W. Xing, H.-J. Wang, Z. Liu, Z.-H. Yu, H.-Y. Zhang and Y. Liu, *Adv. Opt. Mater.*, 2023, 2202588.
13 H.-J. Yu, X.-L. Zhou, X. Dai, F.-F. Shen, Q. Zhou, Y.-M. Zhang, X. Xu and Y. Liu, *Chem. Sci.*, 2022, **13**, 8187–8192.
14 N. A. Thompson, H. Barbero and E. Masson, *Chem. Commun.*, 2019, **55**, 12160–12163.
15 S.-H. Li, X. Xu, Y. Zhou, Q. Zhao and Y. Liu, *Org. Lett.*, 2017, **19**, 6650–6653.
16 Y. H. Ko, K. Kim, J. K. Kang, H. Chun, J. W. Lee, S. Sakamoto, K. Yamaguchi, J. C. Fettinger and K. Kim, *J. Am. Chem. Soc.*, 2004, **126**, 1932–1933.
17 Y. Li, Q. Li, X. Miao, C. Qin, D. Chu and L. Cao, *Angew. Chem., Int. Ed.*, 2021, **60**, 6744–6751.
18 J. Wang, Z. Huang, X. Ma and H. Tian, *Angew. Chem., Int. Ed.*, 2020, **59**, 9928–9933.
19 X.-L. Ni, S. Chen, Y. Yang and Z. Tao, *J. Am. Chem. Soc.*, 2016, **138**, 6177–6183.
20 S. Il Kim, H. Ju Kim and S. Young Park, *Chem*, 2023, **29**, e202203828.
21 N. Barooah, J. Mohanty and A. C. Bhasikuttan, *Chem. Commun.*, 2015, **51**, 13225–13228.
22 H. Liu, M. Lin, Y. Cui, W. Gan, J. Sun, B. Li and Y. Zhao, *Chem. Commun.*, 2021, **57**, 10190–10193.
23 X.-K. Ma, W. Zhang, Z. Liu, H. Zhang, B. Zhang and Y. Liu, *Adv. Mater.*, 2021, **33**, e2007476.
24 H.-J. Wang, W.-W. Xing, H.-Y. Zhang, W.-W. Xu and Y. Liu, *Adv. Opt. Mater.*, 2022, **10**, 2201178.
25 X.-K. Ma and Y. Liu, *Acc. Chem. Res.*, 2021, **54**, 3403–3414.
26 D. Li, F. Lu, J. Wang, W. Hu, X. M. Cao, X. Ma and H. Tian, *J. Am. Chem. Soc.*, 2018, **140**, 1916–1923.
27 Z.-Y. Zhang and Y. Liu, *Chem. Sci.*, 2019, **10**, 7773–7778.
28 Z.-Y. Zhang, W.-W. Xu, W.-S. Xu, J. Niu, X.-H. Sun and Y. Liu, *Angew. Chem., Int. Ed.*, 2020, **59**, 18748–18754.
29 W.-L. Zhou, Y. Chen, Q. Yu, H. Zhang, Z.-X. Liu, X.-Y. Dai, J.-J. Li and Y. Liu, *Nat. Commun.*, 2020, **11**, 4655.
30 D.-A. Xu, Q.-Y. Zhou, X. Dai, X.-K. Ma, Y.-M. Zhang and Y. Liu, *Chin. Chem. Lett.*, 2022, **33**, 851–854.
31 H. Xiang, J. Cheng, X. Ma, X. Zhou and J. J. Chruma, *Chem. Soc. Rev.*, 2013, **42**, 6128–6185.
32 X.-F. Wang, H. Xiao, P.-Z. Chen, Q.-Z. Yang, B. Chen, C.-H. Tung, Y.-Z. Chen and L.-Z. Wu, *J. Am. Chem. Soc.*, 2019, **141**, 5045–5050.
33 X.-M. Chen, Y. Chen, Q. Yu, B.-H. Gu and Y. Liu, *Angew. Chem., Int. Ed.*, 2018, **57**, 12519–12523.
34 S. Garain, B. C. Garain, M. Eswaramoorthy, S. K. Pati and S. J. George, *Angew. Chem., Int. Ed.*, 2021, **60**, 19720–19724.
35 X.-K. Ma, X. Zhou, J. Wu, F.-F. Shen and Y. Liu, *Adv. Sci.*, 2022, **9**, e2201182.

36 E. A. Owens, M. Henary, G. El Fakhri and H. S. Choi, *Acc. Chem. Res.*, 2016, **49**, 1731–1740.
37 A. Bhaskar, G. Ramakrishna, Z. Lu, R. Twieg, J. M. Hales, D. J. Hagan, E. Van Stryland and T. Goodson, *J. Am. Chem. Soc.*, 2006, **128**, 11840–11849.
38 R. Lartia, C. Allain, G. Bordeau, F. Schmidt, C. Fiorini-Debuisschert, F. Charra and M.-P. Teulade-Fichou, *J. Org. Chem.*, 2008, **73**, 1732–1744.
39 Y. Li, S. Liu, H. Ni, H. Zhang, H. Zhang, C. Chuah, C. Ma, K. S. Wong, J. W. Y. Lam, R. T. K. Kwok, J. Qian, X. Lu and B. Z. Tang, *Angew. Chem., Int. Ed.*, 2020, **59**, 12822–12826.
40 H. Xiao, C. Mei, Y. Wang, H. Li, S. Qian, H. Yin and Z. Xu, *Mater. Chem. Phys.*, 2011, **130**, 897–902.
41 L. Wu, J. Liu, P. Li, B. Tang and T. D. James, *Chem. Soc. Rev.*, 2021, **50**, 702–734.